Supporting Information

Heteroporous MoS_2/Ni_3S_2 towards superior electrocatalytic overall urea splitting

Fang Li,[ab] Junxiang Chen,[d] Dafeng Zhang,[ac] Wen-Fu Fu,[*a] Yong Chen,[a] Zhenhai Wen[*d] and Xiao-Jun Lv[*a]

[a] Key Laboratory of Photochemical Conversion and Optoelectronic Materials & CAS-HKU Joint Laboratory on New Materials, Technical Institute of Physics and Chemistry, Chinese Academy of Sciences, Beijing 100190, P.R. China

[b]University of Chinese Academy of Sciences, Beijing 100049, P. R. China

[c]Department of Energy and Chemical Engineering, College of Chemistry and Chemical Engineering, Henan Polytechnic University, Jiaozuo 454003, P. R. China

[d] CAS Key Laboratory of Design and Assembly of Functional Nanostructures, and Fujian Province Key Laboratory of Nanomaterials, Fujian Institute of Research on the Structure of Matter, Chinese Academy of Sciences, Fuzhou, Fujian 350002, China.

Contents:

EXPERIMENTAL SECTION

Materials: All chemicals and solvents were of analytical grade and used as received without further purification. Nickel foam used as the substrate (thickness: 1.8 mm, 100 mm × 100 mm) was purchased from Suzhou Jia Shi De Metal Foam Co., Ltd. Platinum foil was bought from Tianjin AIDA Hengsheng Science-Technology Development Co., Ltd., Ammonium tetrathiomolybdate [$(NH_4)_2MoS_4$, ATM]**,** commercial Pt/C (20 wt %) was purchased from Aladdin Ltd. (Shanghai, China). Urea, Potassium hydroxide, N, N-Dimethylformamide (DMF) and all solvents were obtained from Sinopharm Chemical Reagent Co., Ltd. (Shanghai, China).

Catalyst Preparation. The nickel foams were soaked in acetone to clear away the oil and other oil soluble impurities, followed by immersing them in the dilute HCl (3 M) for about 15 minutes to eliminate the oxide on the surface, washing with deionized water and ethanol three times each, and drying in air for use. The electrodeposition of 3D porous metallic Ni was performed with two-electrode system at the constant current of -0.25 A cm^{-2} for 500 s, Ni foam with a size of 0.5 cm × 0.4 cm as the work electrode and the Pt foil as the counter electrode, the electrolyte was consisted of 2.0 M NH_4Cl and 0.1 M $NiCl_2$, after the deposition, the Ni/NF was cleaned with deionized water and ethanol for several times, followed by drying at room temperature.

The obtained Ni/NF was put in a 25 mL Teflon autoclave, then immersing them with 15 mL DMF containing 80 mg $(NH_4)_2MoS_4$ and then transferring them to the oven and elevating to the reaction temperature of 200 °C for 12 h with a ramping rate of 2 °C per minute. After cooling to the room temperature, the Ni foam with MoS_2 and Ni_3S_2 was cleaned by water and ethanol several times to remove the impurities followed by drying at room temperature. The loading amount of the final catalyst on NF was weighed about ~40.6 mg cm^{-2}. The MoS_2/Ni_3S_2/NF was also prepared using the same method only except that the Ni/NF was substituted by pristine Ni foam. The NF was

immersed into the 15 mL DMF and 100 mg thiourea solution, increasing the oven temperature to 200 ^{o}C and keeping for 12 h to obtain the Ni_3S_2/NF.

Materials Characterization. The Powder XRD analyses were recorded on a diffractometer (Bruker D8 Focus) by using Cu Kα radiation (λ = 1.54056 Å). Scanning electron microscope (SEM) images and elemental mapping were taken on a JSM-7001F field-emission scanning electron microscope operating at 20.0 kV. The concentrations of materials were determined by inductively coupled plasma atom emission spectrometry (ICP-AES, Varian 710-ES, USA). The TEM and HRTEM images were obtained with JEM-2100F equipped with a field emission gun operating at 200 kV. The measurements were performed on a transmission electron microscope (JEM-2100F) operated at an accelerating voltage of 200 kV. X-ray photoelectron spectroscopy (XPS) samples were investigated on a PHI 5300 ESCA system. An Al Kα X-ray source with a power of 250 W was used. The charge effect was calibrated using the binding energy of C 1s (285.0 eV). Raman spectroscopy was carried out on an inVia-Reflex confocal laser micro-Raman spectrometer from 550 cm^{-1} to 250 cm^{-1} using Ar^{+} laser excitation with a wavelength of 532 nm.

Electrochemical Measurements. Electrochemical measurements were performed on a computer-controlled CHI660E electrochemical workstation with a typical three-electrode cell system. The geometrical surface area of the NF electrode used for electrocatalysis was 0.2 cm^2 (0.4 cm × 0.5 cm) and the current density was calculated using the geometrical surface area of 0.4 cm^2. The nickel foam (catalyst loading density ~40.6 mg cm^{-2}) was used as working electrode, an Ag/AgCl (saturated KCl) electrode as the reference electrode, and a Pt foil and graphite rod as the counter electrode for UOR and HER, respectively. The experiments were conducted in an electrolyte solution of 1.0 M KOH (saturated with N_2) and all the potentials reported in our work were quoted with respect to reversible hydrogen electrode (RHE): E (RHE) = E (Ag/AgCl) + 0.197 + 0.059 pH unless stated otherwise. For overall urea splitting, the MoS_2/Ni_3S_2/Ni/NF was used as both the anode and cathode electrodes. The scan rate was

at 5 mV s^{-1}. The electrochemical double layer capacitance (C_{dl}) of the resulting electrocatalysts was evaluated by using cyclic voltammetry in a non-Faradaic region (0.4 − 0.5 V vs RHE for the HER and 1.001 − 1.02 V vs RHE for the UOR) at different scan rates of 10, 30, 50, 70, and 90 mV s^{-1}. Electrochemical impedance spectra for HER was recorded at − 0.2 V vs RHE from 0.1 to 10^6 Hz with an amplitude of 5 mV, and for OER was at 1.6 V vs RHE from 0.001 to 10^6 Hz with an amplitude of 10 mV. As for 20% Pt/C, the catalysts were first dispersed in 1400 μL ethanol and 100 μL of a 5% Nafion mixture solution prior to a ≥30 min sonication to form a homogeneous ink and then loaded the same quality catalysts onto a preprocessed 0.2 cm^2 NF by drop-coating.

Computational Method. Spin-polarized DFT calculations were performed with periodic super-cells under the generalized gradient approximation (GGA) using the Perdew-Burke-Ernzerhof (PBE) functional for exchange-correlation and the ultrasoft pseudopotentials for nuclei and core electrons. The Kohn-Sham orbitals were expanded in a plane-wave basis set with a kinetic energy cutoff of 30 Ry and the charge-density cutoff of 300 Ry. The Fermi-surface effects has been treated by the smearing technique of Methfessel and Paxton, using a smearing parameter of 0.02 Ry. The sideviews of edge MoS_2 and slab NiO(010) are depicted on Fig. S17a and b. All atoms on MoS_2 model and two topmost layers of NiO are allowed to relax during the structure optimization until the Cartesian force components acting on each atom were below 10^{-3} Ry/Bohr and the total energy converged to within 10^{-5} Ry. The Brillouin-zones were sampled with 5×5×1 and 1×2×1 k-point mesh for NiO and MoS_2. The PWSCF codes contained in the Quantum ESPRESSO distribution[1] were used to implement the calculations. The optimized structures of CO* and NH* on edge MoS_2 and NiO are depicted on Fig. S17c and d. Other details about the method to calculate the reaction free energies are the same as our former paper.[2]

The key intermediates during the UOR should be NH* and CO*, which are formed through the cracking of the C-N bond in urea, and we consider a simplified reaction UOR mechanism, where the asterisks denote adsorption species:

$$CO(NH_2)_2(aq) \rightarrow CO(NH_2)_2* \quad \text{(S1)}$$

$$CO(NH_2)_2*+2OH^- \rightarrow CO*+2NH* + 2H_2O(l) + 2e^- \quad \text{(S2)}$$

$$CO* + 2NH*+ 4OH^- \rightarrow CO_2(g) + N_2(g) +3H_2O(l) + 4e^- \quad \text{(S3)}$$

Eqn (S1) corresponds to the adsorption of urea on the surface of catalysts. Eqn (S2) corresponds to the dissociation of adsorbed urea, whereby the cracking of its C-N bond leads to the formation of NH* and CO* and causes the transfer of two electrons. Eqn (S3) corresponds to the further oxidation of NH* and CO*, which eventually forms CO_2 and N_2. On the basis of Eqn (S1)-(S3), reaction free energy diagrams (FEDs) of the UOR of MoS_2 and Ni_3S_2 are calculated and depicted in Fig. 4a. Fig. 4a indicates that for both catalysts the dissociative adsorption of urea is exothermic, indicating that a more favorable adsorption of CO* and NH* can increase UOR performance by lowering the thermodynamic barrier of the UOR (represented by the bidirectional arrows in Fig. 4a).

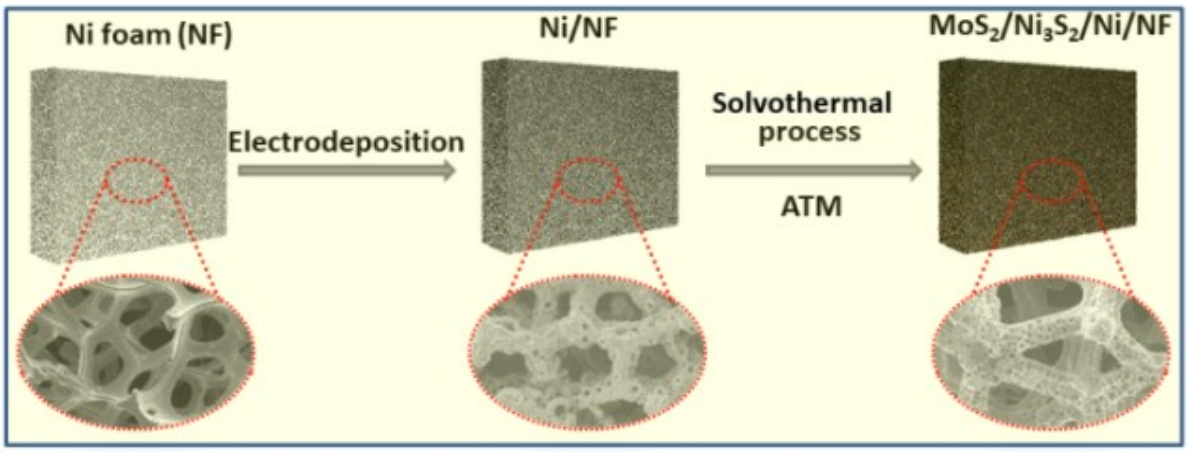

Scheme 1 Preparation process of heteroporous MoS_2/Ni_3S_2/Ni/NF

The hierarchically heteroporous MoS_2/Ni_3S_2 catalyst was synthesized by two steps (**Scheme 1**). The macroporous metallic nickel layer was firstly electrodeposited on Ni foam (NF). The obtained porous Ni/NF further reacted with $(NH_4)_2MoS_4$ (ATM) under solvothermal conditions to form the MoS_2/Ni_3S_2 heterostructure.

RESULTS:

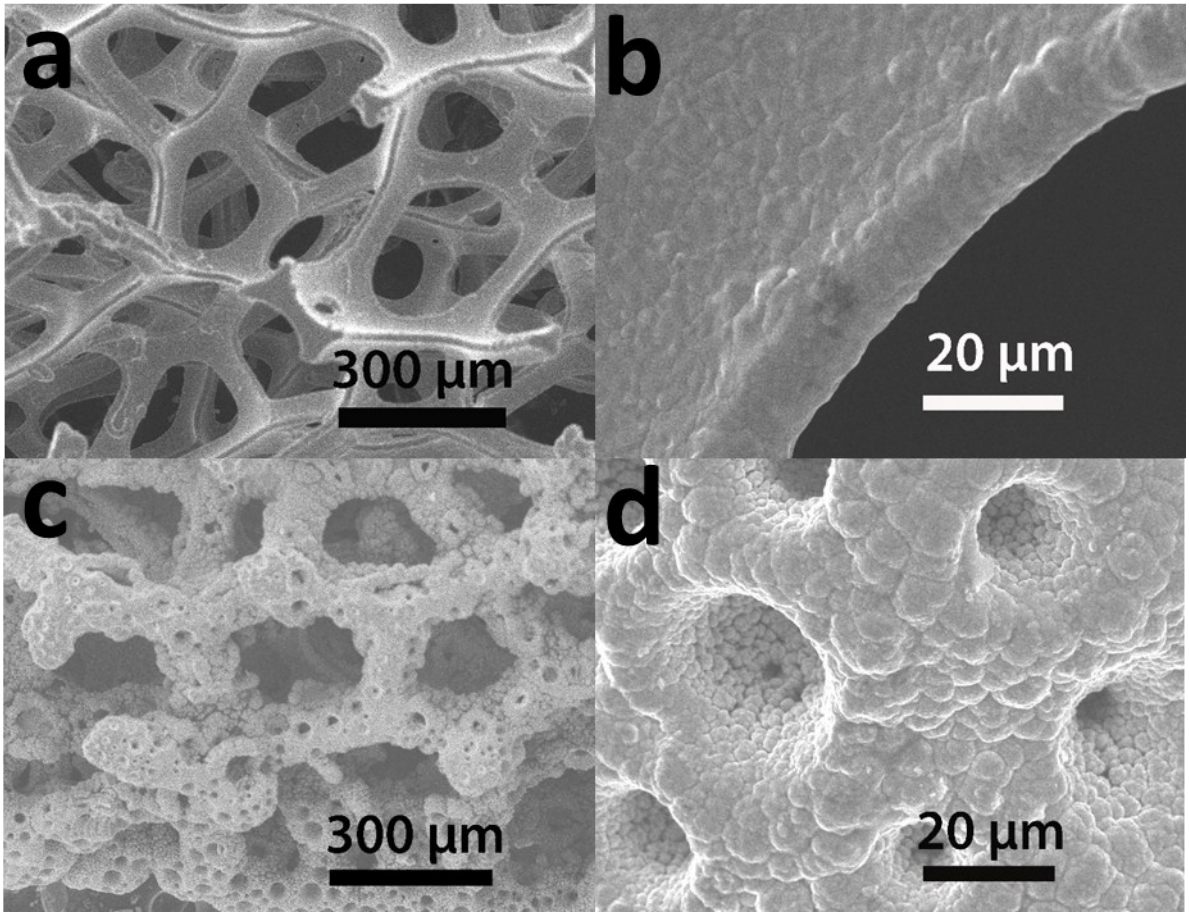

Fig. S1 (a, b) SEM images of the Ni Foam, (c, d) SEM images of the electrodeposited porous Ni/NF at different maginifications

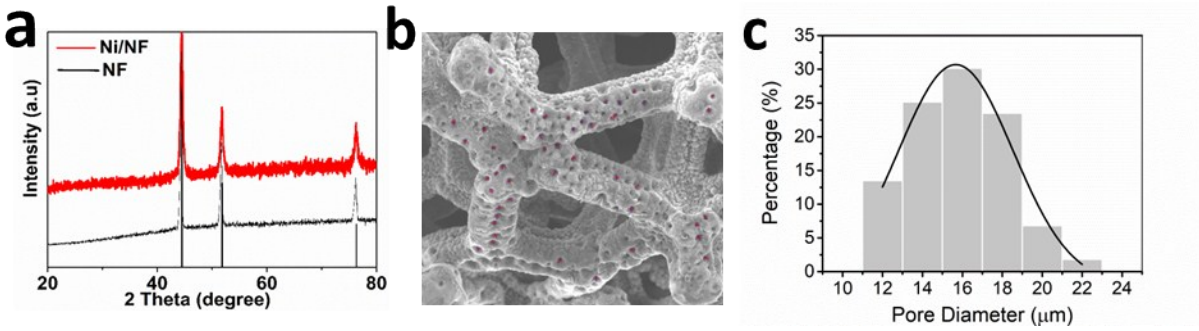

Fig. S2 (a)The X-ray diffraction (XRD) pattern of metallic nickel before and after electrodeposition on the Ni form. (b) and (c) the distribution of the pore diameter

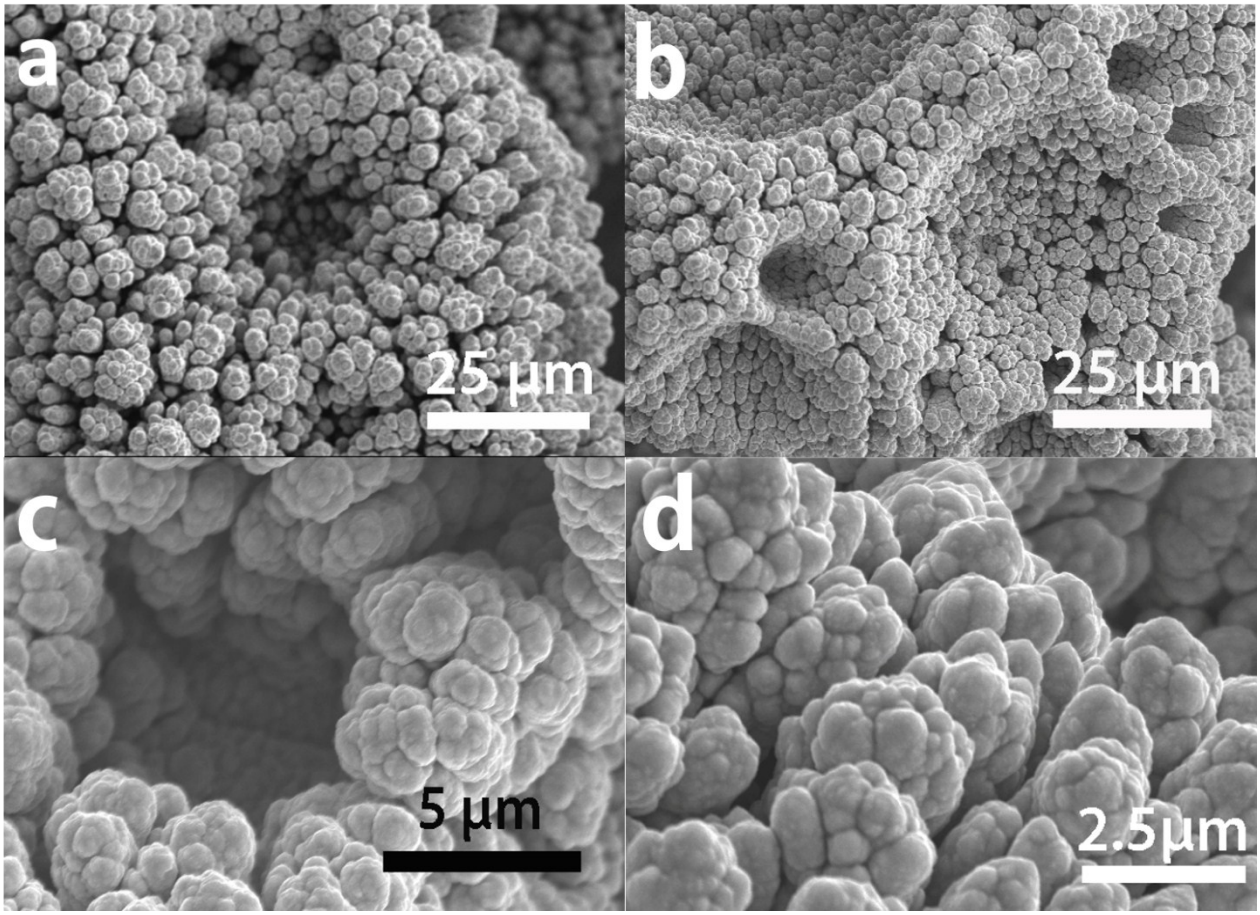

Fig. S3 (a, b, c, d) SEM images of the porous structure after electrodeposited Ni on Ni form at different maginifications.

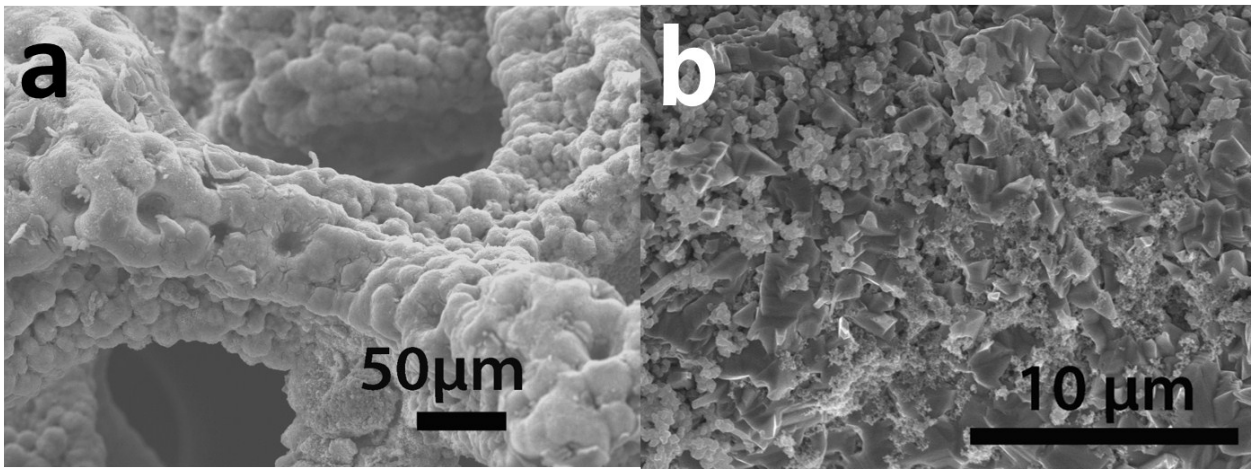

Fig. S4 (a, b) SEM images of the $MoS_2/Ni_3S_2/Ni/NF$.

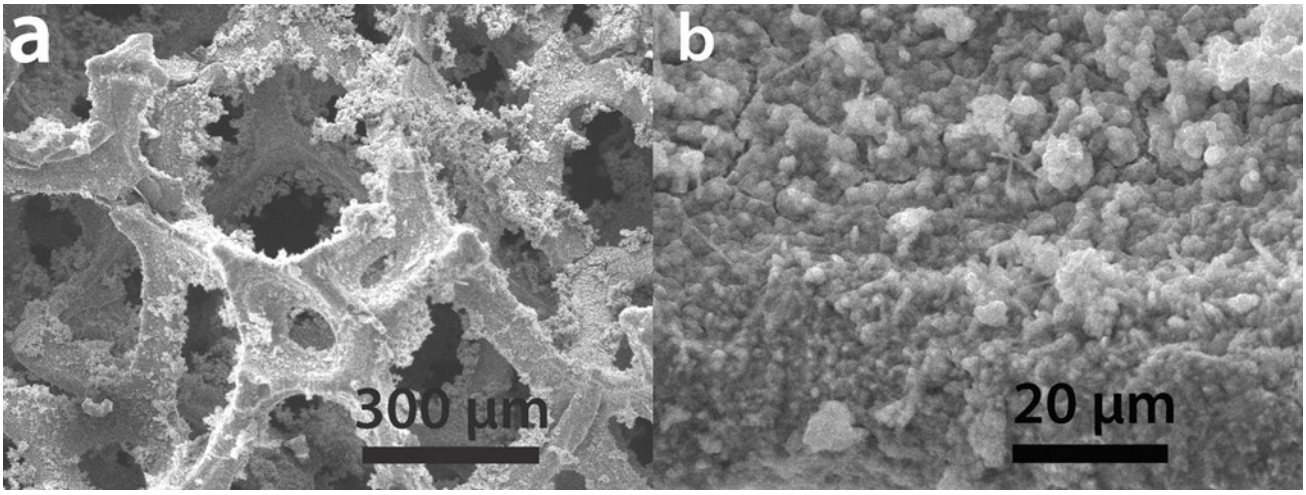

Fig. S5 (a, b) SEM images of the MoS_2/Ni_3S_2/NF.

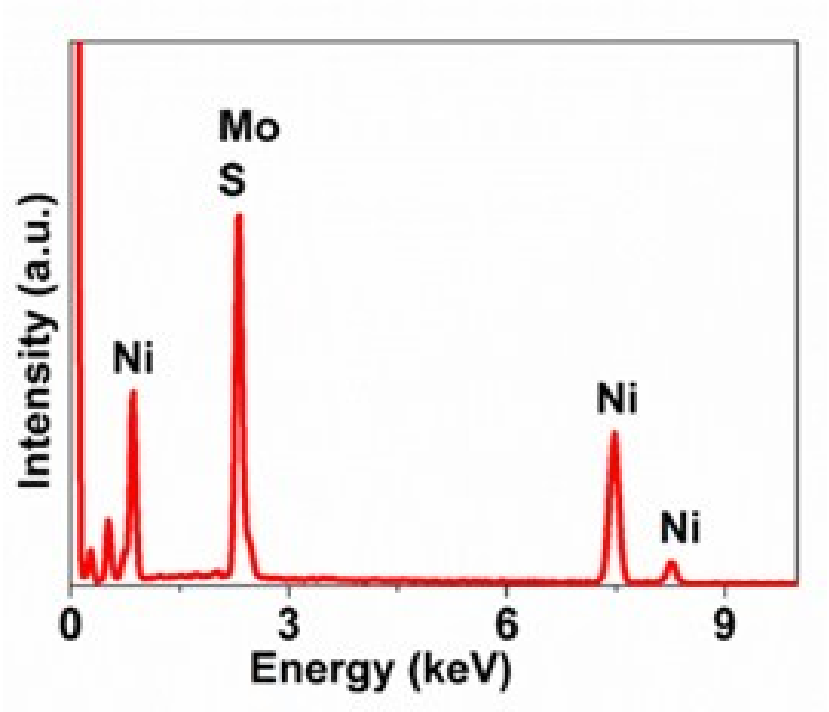

Fig. S6 Energy dispersive spectrum of the MoS_2/Ni_3S_2/Ni/NF.

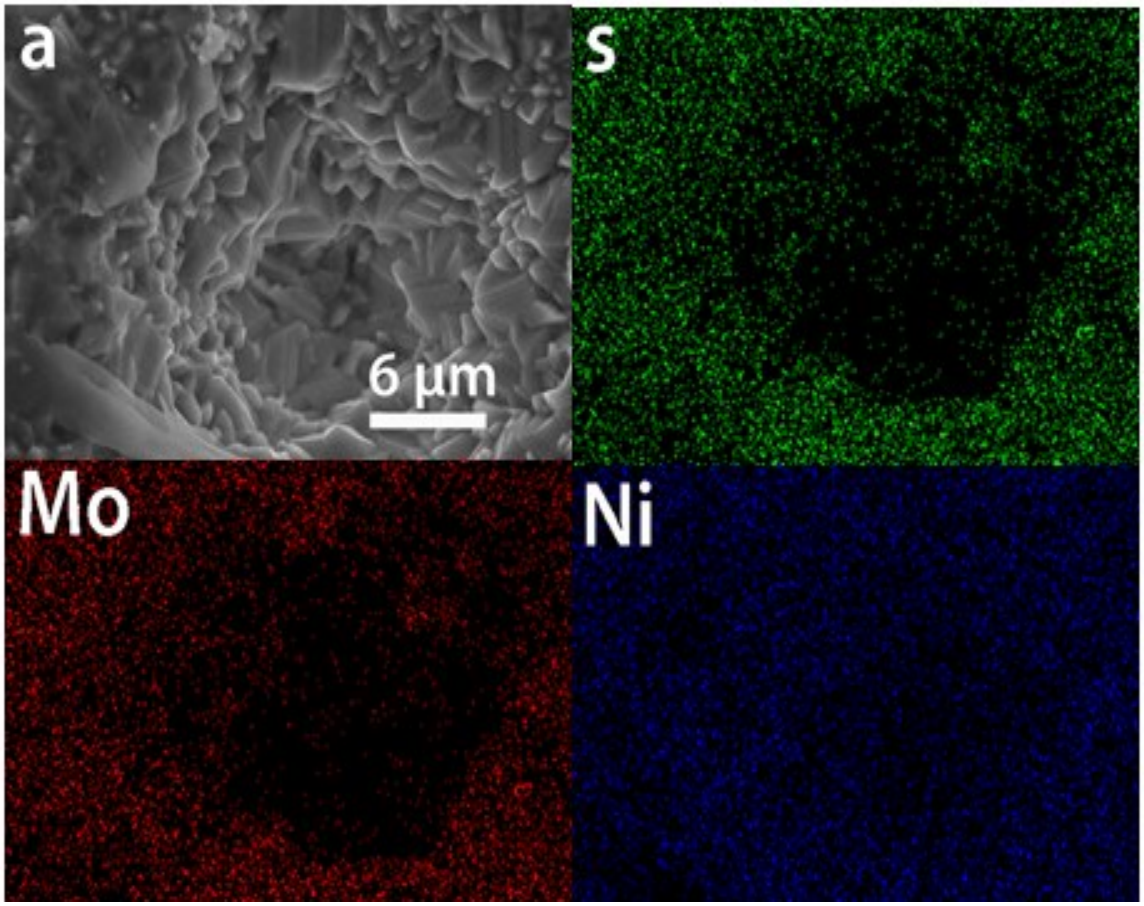

Fig. S7 (a) SEM image of the porous structure $MoS_2/Ni_3S_2/Ni/NF$ and the mapping of the S, Mo, and Ni which demonstrate the existence of S, Mo, and Ni and the uniform distribution in the pore.

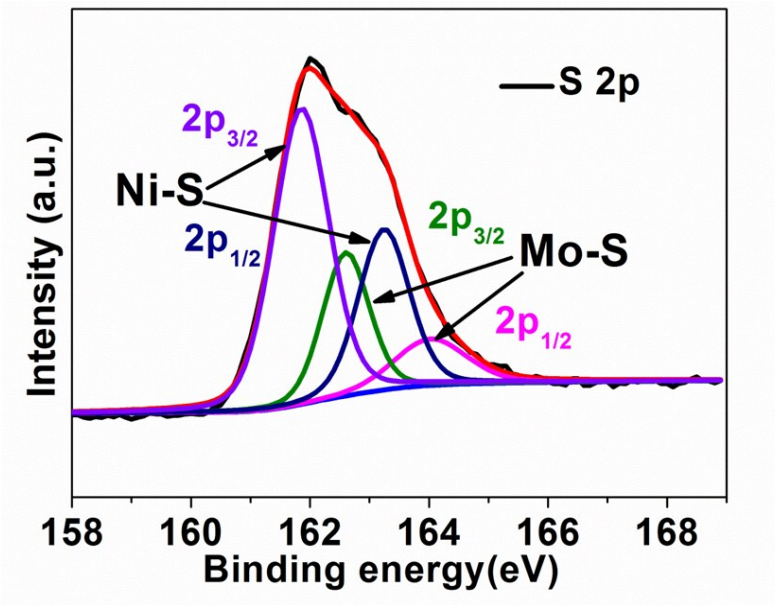

Fig. S8 XPS profile of S 2p, including the Ni-S bond ($2p_{1/2}$ and $2p_{3/2}$) and Mo-S bond ($2p_{1/2}$ and $2p_{3/2}$).

The positive shift means the valence state of the metals are more positive, and further demonstrate the change of the charge density in MoS_2/Ni_3S_2 compound in comparison with the pure MoS_2 and Ni_3S_2. On one hand, the change of the binding energy declares that MoS_2 and Ni_3S_2 exist the electronic interact of each other. The electronic interconnection is advantage for the charge transfer of the electrocatalysis. On the other hand, the positive shifts mean the metal can expose more empty d-ordits which provide more absorbance sites for the intermediate for the improvement of the electrocatalysis. (*Angew. Chem. Int. Ed.*, 2016, **55**, 6702., *ACS Catal.*, 2017, **7**, 2357.)

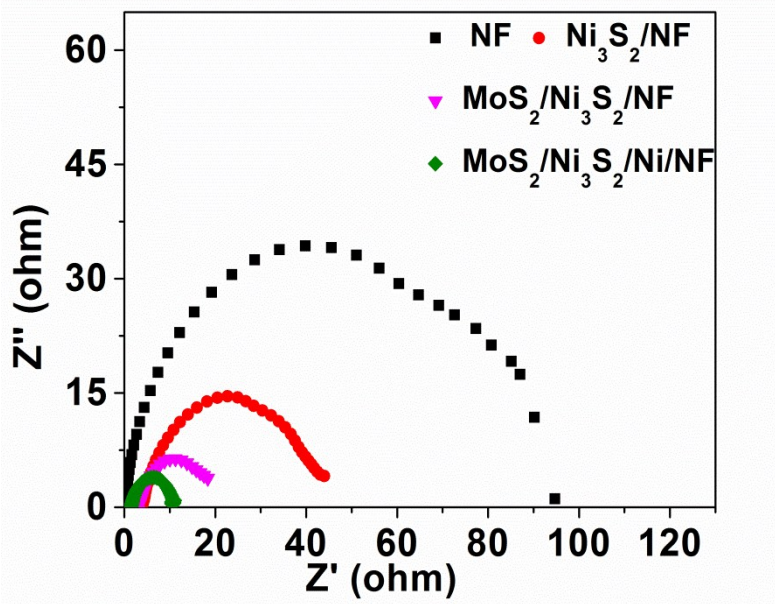

Fig. S9 Electrochemical impedance spectroscopy of MoS_2/Ni_3S_2/Ni/NF, MoS_2/Ni_3S_2/NF, Ni_3S_2/NF and NF for UOR.

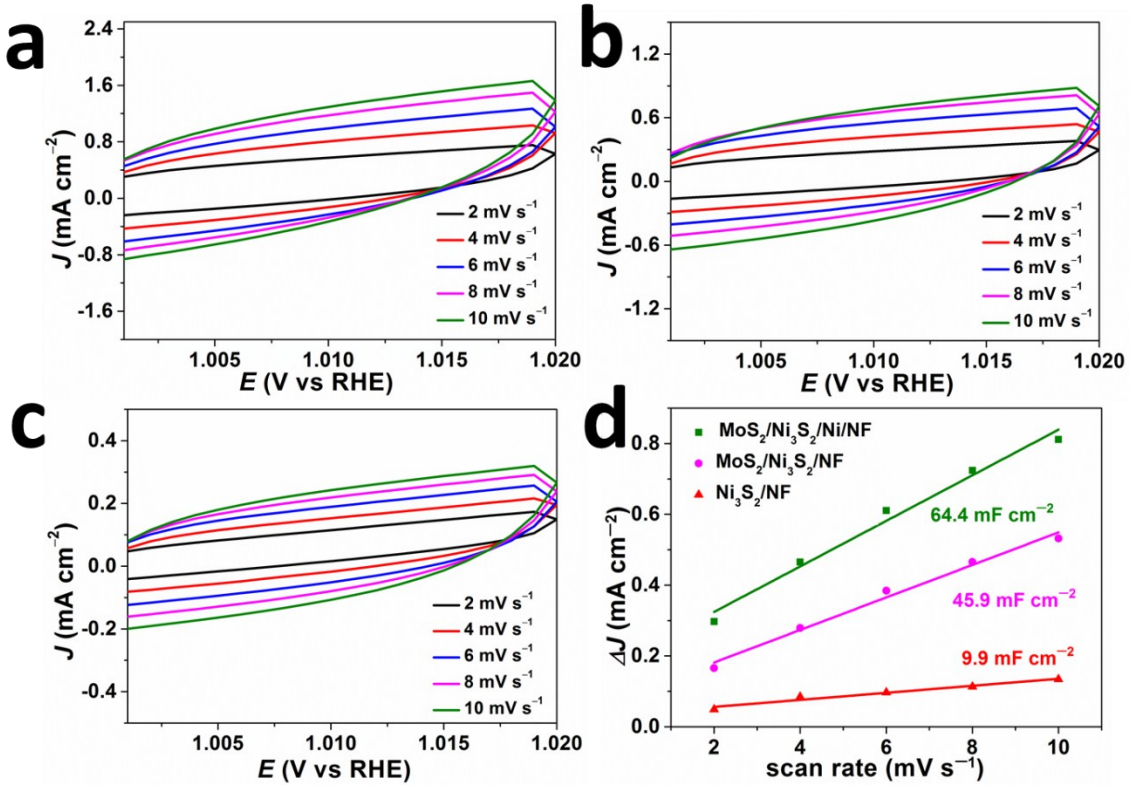

Fig. S10 Cyclic voltammetry for (a) $MoS_2/Ni_3S_2/Ni/NF$, (b) $MoS_2/Ni_3S_2/NF$ and (c) Ni_3S_2/NF in a non-Faradaic region of the potential range from 1.00 – 1.02 V *vs* RHE at scan rate from 2 to 10 mV s^{-1} measured in 1.0 M KOH solution with 0.33 M urea. (d) The calculated C_{dl} .The current density at the potential of the 1.01 V *vs* RHE ploted with the scan rates.

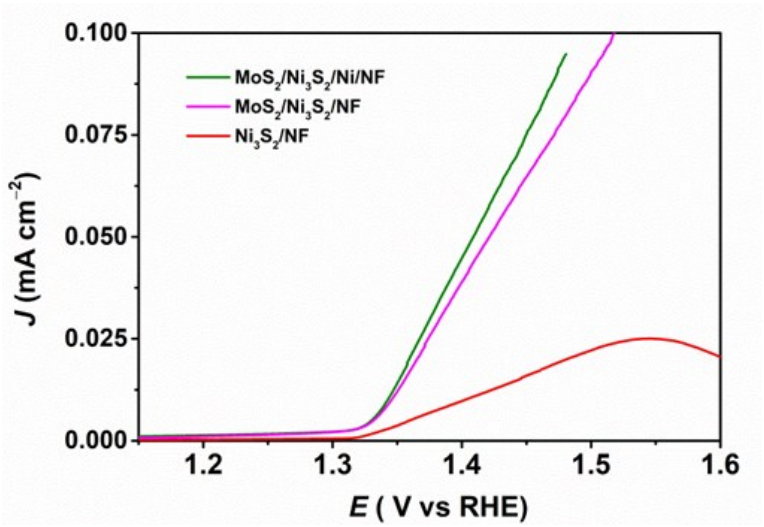

Fig. S11 The intrinsic current density of the heteroporous MoS_2/Ni_3S_2, MoS_2/Ni_3S_2/NF and Ni_3S_2/NF. The specific OER activity is calculated via normalizing the current by the corresponding ECSA. The ECSA is determined via dividing C_{dl} by 40 μF cm^{-2}.

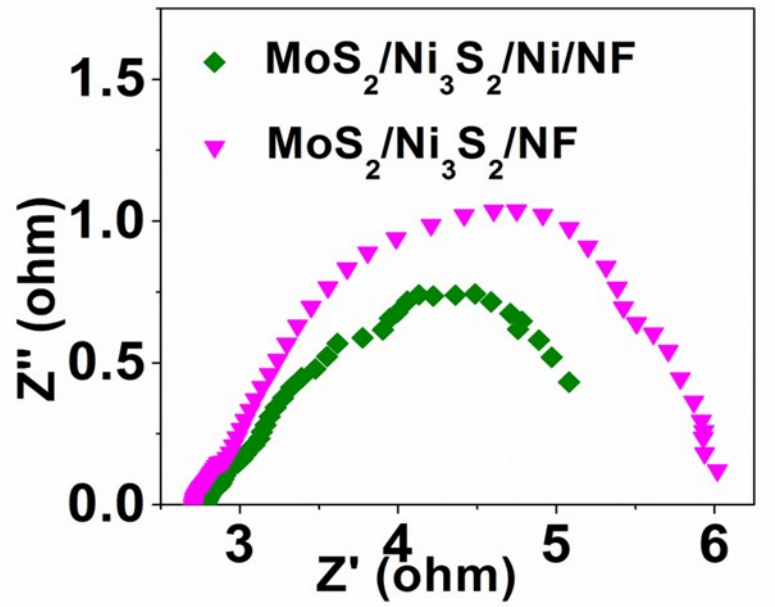

Fig. S12 the Nyquist plots of MoS_2/Ni_3S_2/Ni/NF and MoS_2/Ni_3S_2/NF.

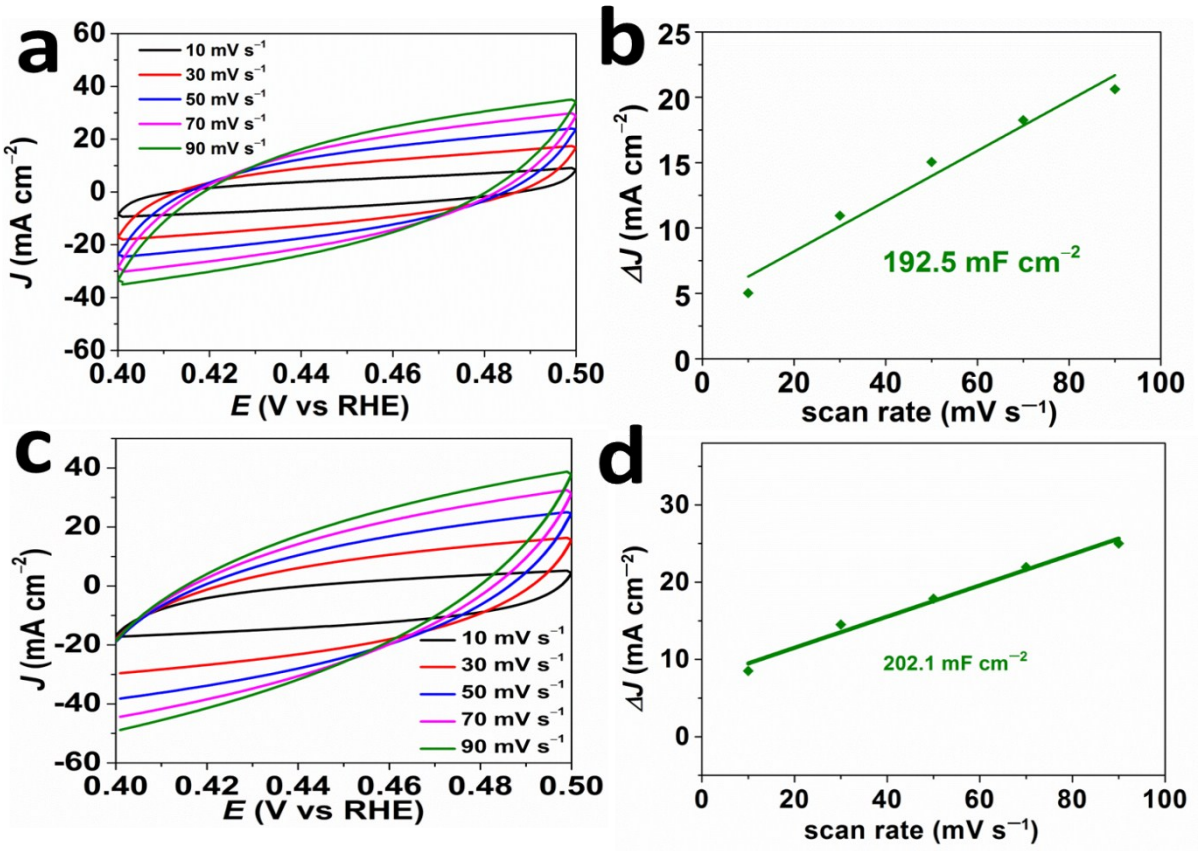

Fig. S13 Cyclic voltammetry for (a) $MoS_2/Ni_3S_2/Ni/NF$ in a non-Faradaic region of the potential range from 0.4 V– 0.5 V *vs* RHE at scan rate from 10 to 90 mV s^{-1} measured in 1.0 M KOH solution with 0.33 M urea. (b) The calculated C_{dl} .The current density at the potential of the 0.45 V *vs* RHE ploted with the scan rates. (c) Cyclic voltammetry for (a) $MoS_2/Ni_3S_2/Ni/NF$ in a non-Faradaic region of the potential range from 0.4 V– 0.5 V *vs* RHE at scan rate from 10 to 90 mV s^{-1} measured in 1.0 M KOH solution. (d) The calculated C_{dl} in blank KOH solution. The current density at the potential of the 0.45 V *vs* RHE ploted with the scan rates.

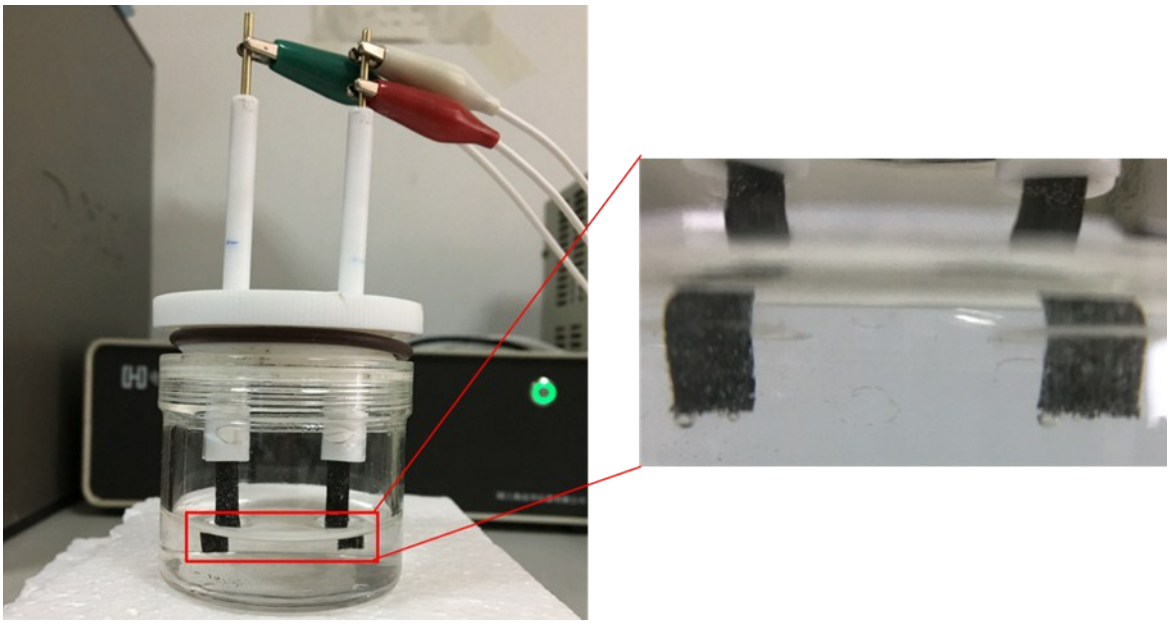

Fig. S14 The optical photograph of the setup during the overall urea splitting. The electrolyte was 1.0 M KOH with 0.33 M urea. The MoS_2/Ni_3S_2/Ni/NF was used as cathode and anode at the same time.

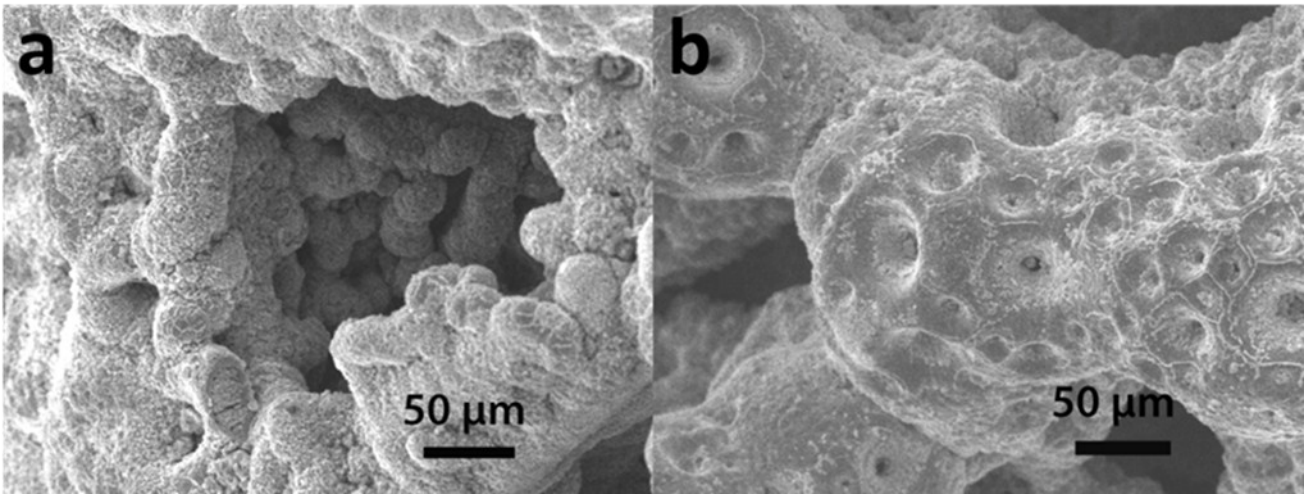

Fig. S15 (a) SEM image of MoS_2/Ni_3S_2/Ni/NF after HER. (b) The SEM image of MoS_2/Ni_3S_2/Ni/NF after UOR. The porous morphology of the MoS_2/Ni_3S_2/Ni/NF maintained very well.

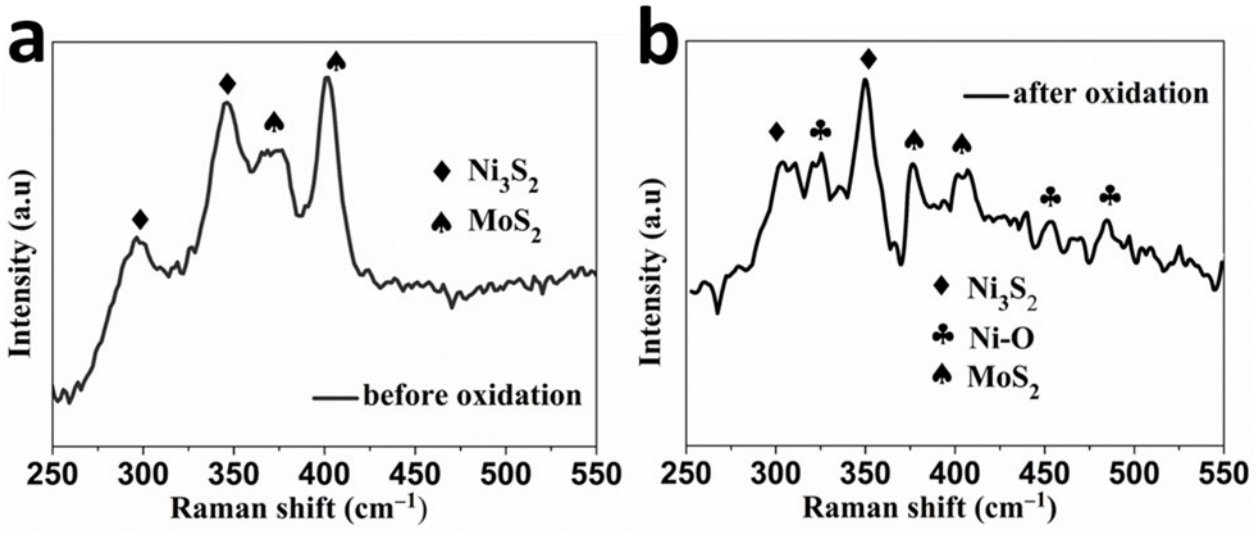

Fig. S16 (a) The Raman spectrum of the $MoS_2/Ni_3S_2/Ni/NF$ before the UOR. (b) The Raman spectrum of the $MoS_2/Ni_3S_2/Ni/NF$ after long term UOR.

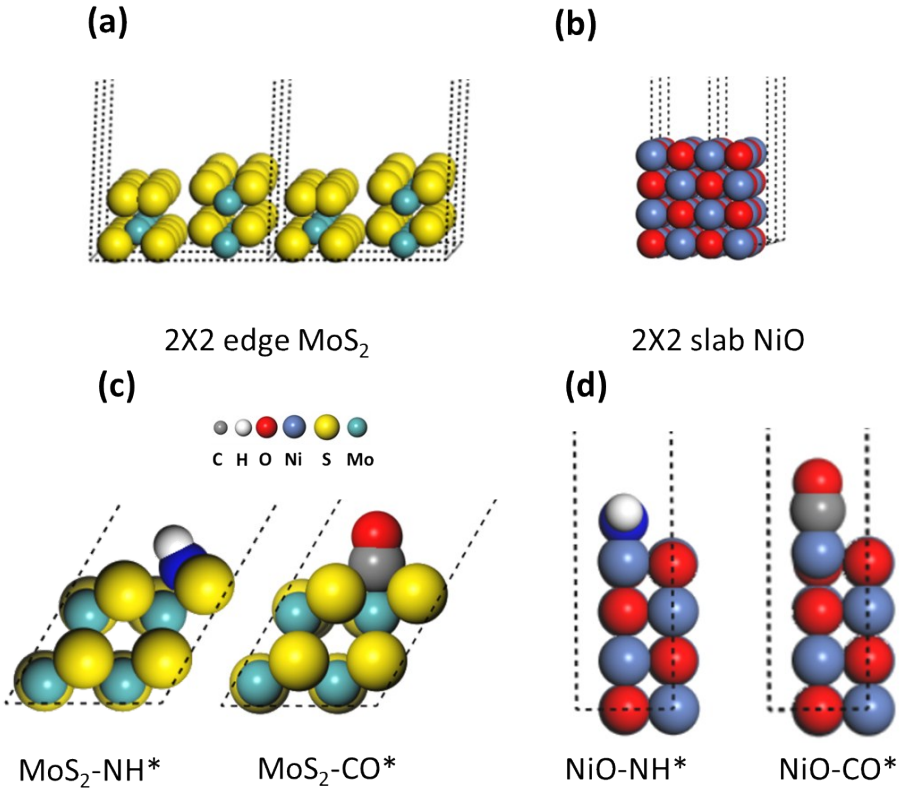

Fig. S17 (a-b) The DFT models of MoS_2 and NiO, where (a) shows the edge model of MoS_2, and (b) shows the slab model of NiO. (c-d) The optimized NH* and CO* and MoS_2 and NiO.

Table S1. Comparative activity summary of urea conversion for several recently reported highly active catalysts.

Catalysts	UOR		Overall urea splitting		Refs
	Potential @10 (mA cm^{-2})(V *vs* .RHE)	Potential @50 (mA cm^{-2})(V *vs* .RHE)	Potential @10 (mA cm^{-2})(V *vs* .RHE)	Potential @20 (mA cm^{-2})(V *vs* .RHE)	
MoS_2/Ni_3S_2/Ni/NF	1.24	1.33 (200 mA cm^{-2})	1.38	1.5248	This work
MoS_2/Ni_3S_2/NF	1.29	1.36 (200 mA cm^{-2})	1.45	1.58	This work
Ni_3S_2/NF	1.32	1.38 (200 mA cm-2)	1.58	1.7	This work
Pt/C	1.36	1.44 (200 mA cm-2)	1.53	1.63	This work
NiMoS		1.38	1.59		*Nano Research* **2017**, https://doi.org/10.1007/s12274-017-1711-3
3D $Ni(OH)_2$ Nanotube-NF	1.41				*Electrochem. Commun.*, 2013, 29, 21
S-MnO_2	1.33		1.41		*Angew. Chem. Int. Ed.* **2016**, *55* , 3804−3808
L-MnO_2	1.37				*Angew. Chem. Int. Ed.* **2016**, *55* , 3804−3808
Pt/C	1.48		1.68		*Angew. Chem. Int. Ed.* **2016**, *55* , 3804−3808
NiO nanosheet	1.38				*J. Power Sources,* **2014**, *272* , 711−718
$MnO_2/MnCo_2O_4$/Ni	1.33		1.58	1.75	*J. Mater. Chem.* A, **2017**, *5* , 7825−7832
NiMo sheet array	1.37				*Electrochem. Acta* , 2015, 153, 456−460

Table S2. A comparative summary of HER activities

Catalysts	Electrolyte	J (mA cm^{-2})	overpotential (mV)	Tafel slope (mV dec^{-1})	Refs
MoS_2/Ni_3S_2/ Ni/NF	1 M KOH with 0.33M urea	10	99	67	this work
$MoS_2/CoSe_2$	0.5M H_2SO_4	10	68	36	Nat. commun. 2015, 6.
Ni2.3%CoS_2 /CC	1 M KOH	10	150	106	Electrochem. Commun. 2016, 63, 60−64
Ni_3S_2/Ni	1 M KOH	10	195	107	Electrochim. Acta 2015, 174, 297−301
NiS_2-MoS_2	1 M KOH	400	400	70	*J. Mater. Chem. A 2016, 4, 13439−13443*
$CoMoS_3$	0.5M H_2SO_4	10	171	56.9	*Adv. Mater. 2016, 28, 92−97*
hollow MoS_2	0.5M H_2SO_4	10	214	74	ACS Appl. Mater. Interfaces 2016, 8, 5517−5525
MoS_2/RGO	0.5M H_2SO_4	10	100	41	*J. Am. Chem. Soc. 2011, 133, 7296−7299*
NiS_2	1 M KOH	10	148	79	*ACS Appl. Mater. Interfaces 2017, 9, 2500−2508*
Ni_3S_2-NGQDs/NF	1 M KOH	10	218	89	*Small 2017*
Ni-Co/1T phase MoS_2	1 M KOH	10	70	38.1	*Nat. Commun. 2017, 8, 15377−15387*
Ni_3S_2/NF	1 M KOH	10	260		*J. Am. Chem. Soc. 2015, 137, 14023−14026*
Ni_5P_4	1 M KOH	10	150	53	*Angew. Chem., Int. Ed. 2015, 127, 12538−12542*
MoO_x/Ni_3S_2	1 M KOH	10	106	90	*Adv. Funct. Mater. 2016, 26, 4839−4847*
$Ni_xCo_{3-x}S_4$/ Ni_3S_2/NF	1 M KOH	10	136	107	Nano Energy 2017, 35, 161−170
Co_9S_8/MoS_2/ CNFs	0.5M H_2SO_4	10	190	110	*Adv. Mater. 2015, 27, 4752−4759*

REFERENCES:

(1) Giannozzi,P.; Bonini, S. B. N.; Calandra, M; Car, R.; Cavazzoni, C.; Ceresoli, D.; Chiarotti, G. L.; Cococcioni, M.; Dabo, I.; Dal Corso, A.; Fabris, S.; Fratesi, G.; de Gironcoli, S.; Gebauer, R.; Gerstmann, U.; Gougoussis, C.; Kokalj, A.; Lazzeri, M.; MartinSamos, L.; Marzari, N.; Mauri, F.; Mazzarello, R.; Paolini, S.; Pasquarello, A.; Paulatto, L.; Sbraccia, C.; Scandolo, S.; Sclauzero, G.; Seitsonen, A. P.; Smogunov, A.; Umari, P.; Wentzcovitch, R. M. QUANTUM ESPRESSO: a modular and open-source software project for quantum simulations of materials. *J. Phys.: Condens. Matter* **2009**, 21, 395502

(2) G. Wang, J. Chen, Y. Li, J. Jia, P. Cai and Z. Wen, *Chem. Commun.* **2018**, DOI: 10.1039/C7CC09653D.